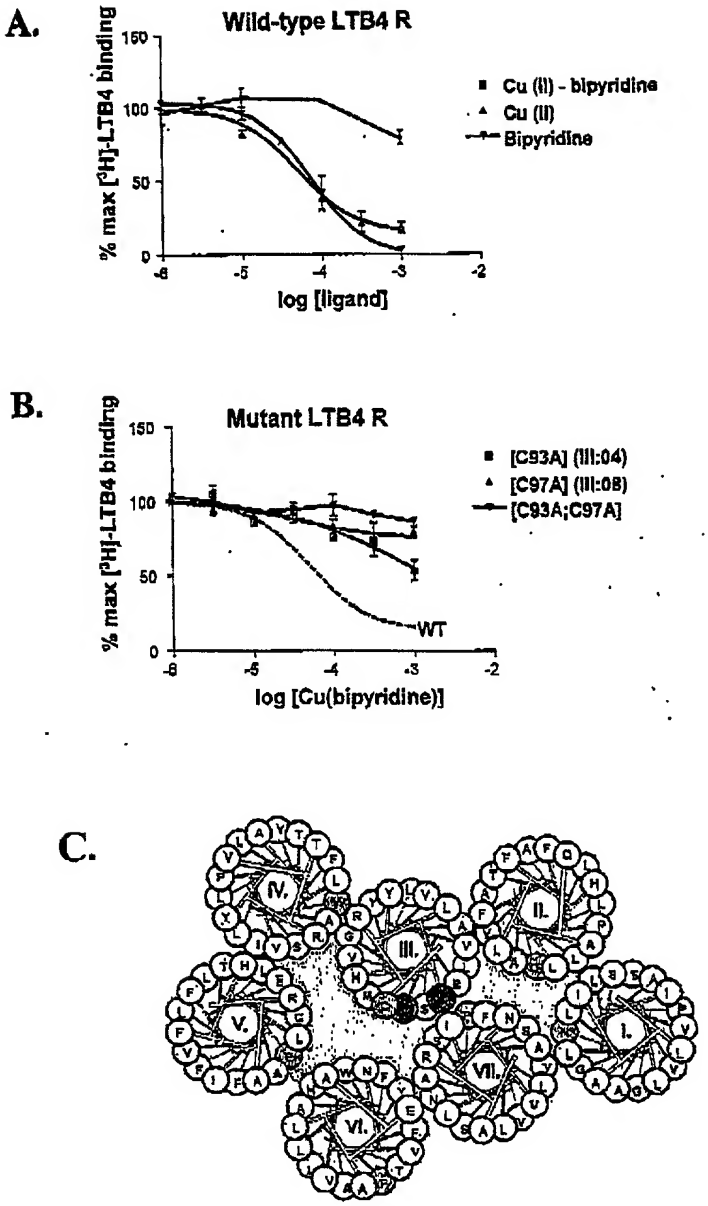

Fig I.1

Identification of naturally occurring metal-ion binding site in the 7TM leukotriene LTB4 receptor

Whole cell competition binding experiment with COS-7 cells expressing the wild type and mutant variants of the leukotriene LTB4 receptor using [^{3}H]-LTB4 as the radioligand.

Panel A. Affinity of Cu(II), 2,2'-bipyridine and the complex therof in the wild type LTB4 receptor.

Panel B. Affinity of Cu(bipyridine) in mutant forms of the LTB4 receptor in which the metal-ion binding is severely imparired.

Panel C.Helical wheel diagram illustrating the transmembrane segments of the LTB4 receptor. The two cysteine residues within the transmembrane segment III which have been identified as critical for metal-ion chelator complex binding, Cys93 and Cys97 are indicated in dark gray.

A.

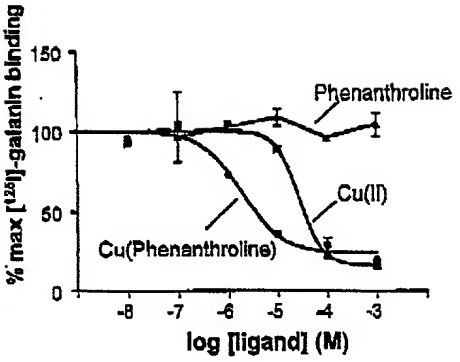

B.

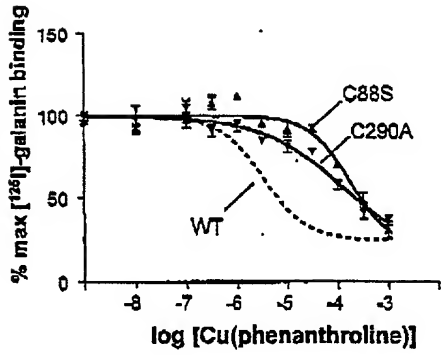

Fig I.2

Identification of naturally occurring metal-ion binding site in the 7TM galanin receptor

Whole cell competition binding experiment with COS-7 cells expressing the wild type and mutant forms of the galanin receptor using [^{125}I]-galanin as radioligand.

Panel A. Affinity of the free copper metal-ion, the free chelator and the phenanthroline complex on the wild-type galanin receptor.

Panel B. Affinity of the copper-phenanthroline copmplex on two mutant forms of the galanin receptor, in which the binding of the metal-ion complex is impaired.

A.

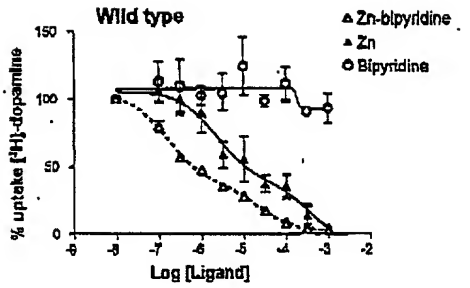

B.

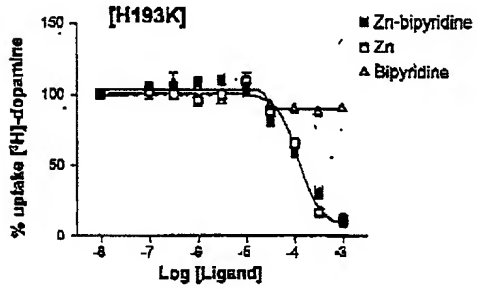

C.

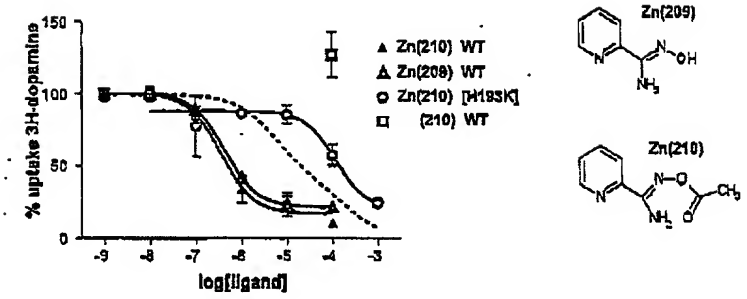

Fig I.3

Identification of naturally occurring metal-ion binding site in the 12TM protein, the dopamine transporter.

Competition analysis of uptake of [^{3}H]-dopamine in whole COS-7 cells expressing the dopamine transporter.

Panel A. Uptake of [^{3}H]-dopamine by the wild-type dopamine transporter in the presence of free metal zinc-ion and zinc in complex with the chelator 2,2'-bipyridine.

Panel B. Dopamine uptake analysis in a mutant form of the dopamine transporter, [H193K], in which binding of the metal-ion complex has been eliminated (Noregaard et al. EMBO J. (1998) 17: 4266-4273).

Panel C. Effect of metal-ion complex formation on the ability to inhibit [^{3}H]-dopamine uptake in the wild-type and [H193K] mutant dopamine transporter. (For compounds, 209 and 210, see list of compounds in Appendix).

A.

		Ions				1,10-Phenanthroline-complexes				2,2'-Bipyridine-complexes			
		Zn	± SEM (n)	Cu	± SEM (n)	Zn	± SEM (n)	Cu	± SEM (n)	Zn	± SEM (n)	Cu	± SEM (n)
WT hNK 1		320	± 20 (5)	370	± 30 (5)	490	± 50 (4)	480	± 60 (3)	390	± 60 (4)	150	± 30 (2)
Y92H	II:24;III:04	17	± 3 (3)	28	± 5 (2)	26	± 5 (2)	28	± 6 (3)	31	± 5 (3)	25	± 3 (2)
E193H:N109H	III:05;V:01	13	± 5 (2)	120	± 20 (2)	46	± 9 (2)	120	± 20 (2)	13	± 4 (2)	160	± 30 (2)
P112H;M291C	III:06;VII:06	41	± 9 (6)	82	± 15 (2)	63	± 4 (5)	45	± 12 (4)	21	± 2 (4)	13	± 2 (4)
Y272H	V:05;VI:24	9.1	± 1 (3)	330	± 50 (3)	6.6	± 1.2 (3)	150	± 20 (2)	9.6	± 3.2 (2)	140	± 20 (2)

B.

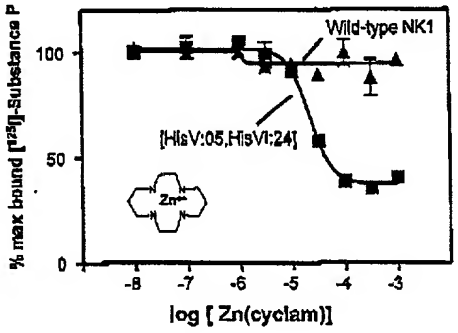

C.

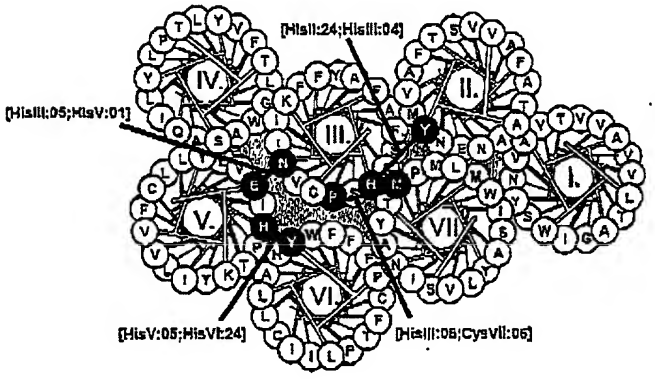

Fig II.1

Binding of various metal-ion complexes to a library of inter-helical metal-ion sites engineered into the tachykinin NK1 receptor.

COS-7 cells expressing various engineered forms of the NK1 receptor were analyzed by competition binding using [^{125}I]-Substance P as radioligand.

Panel A. IC_{50} values for the zinc and copper metal-ions and complexes thereof with the chelators, 2,2'-bipyridine and phenanthroline are presented in the table. N indicated the number of experiments performed.

Panel B. Data obtained using the chelator cyclam are presented for the NK1 mutant in which an inter-helical metal-ion site has been generated through the introduction of the HisV:05;HisVI:24 exchanges.

Panel C. A helical diagram representing the four sets of inter-helical metal-ion sites which appear in Panel A are indicated.

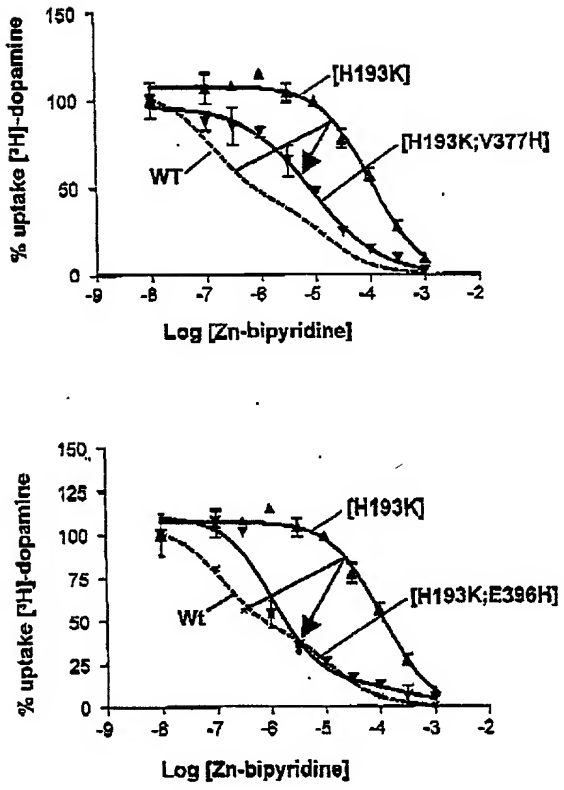

Fig IL2 Re-engineering of a metal-ion chelator binding site in the 12TM dopamine transporter. Dopamine uptake was analysed in COS-7 cells expressing the wild type and mutant forms of the dopamine transporter in competition with the metal-ion chelator complex, zinc(II)-2,2'-bipyridine. The two panels show two forms of re-engineered dopamine transporters in which the ability to bind the metal-ion chelator complexes have been reconstituted following the elimination of the His193 interaction point.

A.

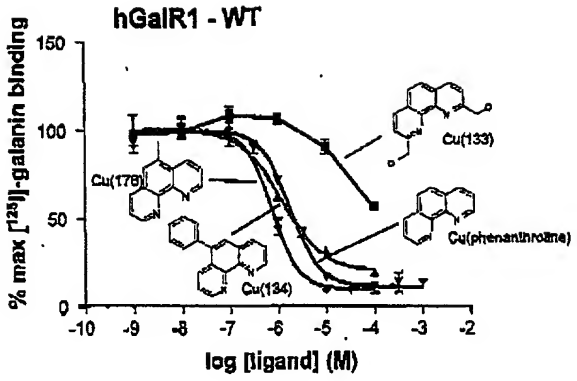

B.

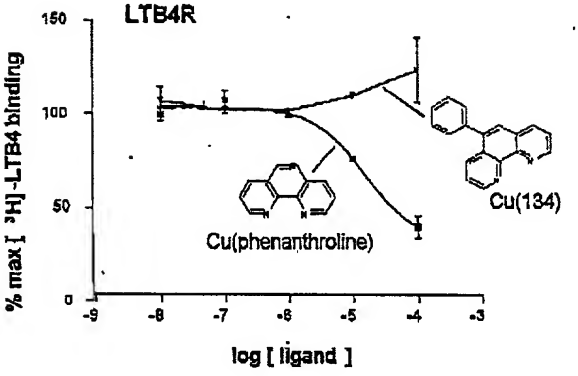

Fig III.1

Structure-activity relationship of antagonist metal-ion complexes in the galanin and the leukotriene LTB4 receptors.

Panel A. Competition binding analysis in COS-7 cells expressing the galanin receptor. Binding of [^{125}I]-galanin was analysed in the presence of various copper-ion chelator complexes.

Panel B. Competition binding analysis in COS-7 cells expressing the LTB4 receptor. Binding of [^{3}H]-LTB4 was analysed in the presence of various copper-ion chelator complexes.

For structures of the chelators employed in both panels, see Appendix.

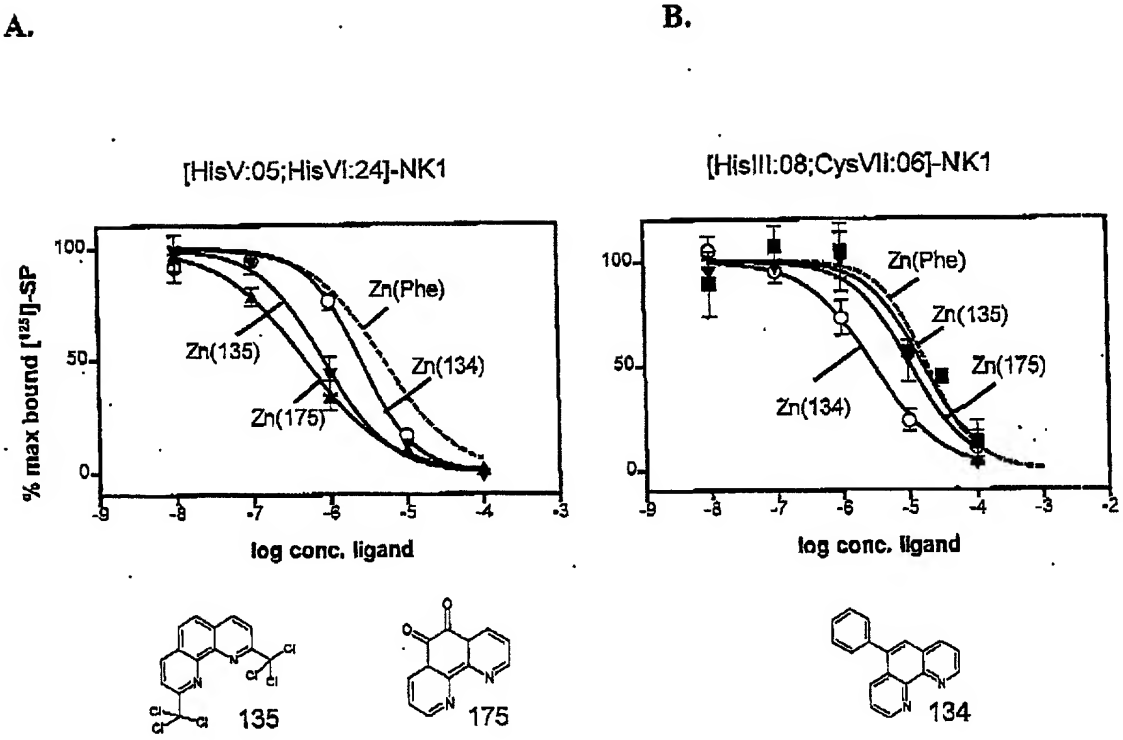

Figur III.2
Structure-activity relationship of antagonist metal-ion complexes in the metal-ion site engineered tachykinin NK1 receptor
Binding of [^{125}I]-Substance P was analysed in COS-7 cells expressing NK1 receptor which have been engineered to bind the zinc metal-ion. Ligand binding is presented in competiton with the zinc metal-ion, the zinc-1,10-phenanthroline complex and with other zinc-chelator xomplexes as indicated. For structures of the chelators, see Appendix.

A.

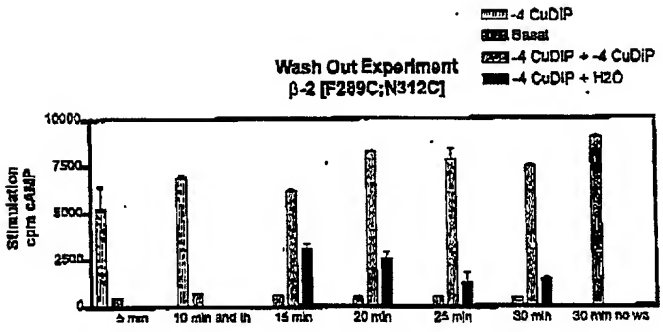

B.

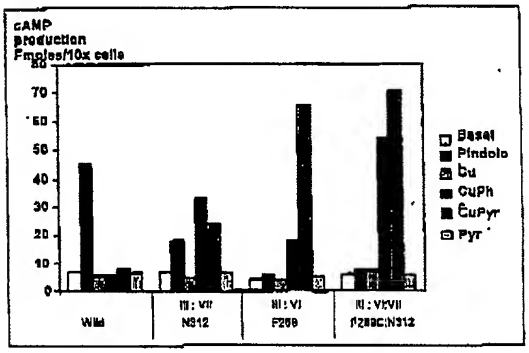

C.

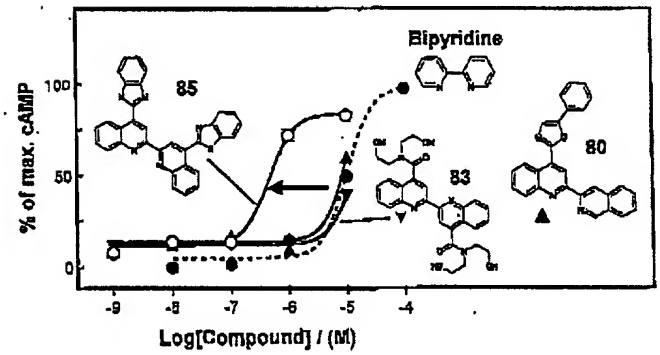

Figur III.3

Structure-activity relation ship of agonistic metal-ion complexes in the metal-ion site Beta2-adrenergic receptor.

The effect of Cu(II) and copper-chelator complexes on stimulation of accumulation of intracellular cAMP was analyzed in COS-7 cells expressing the beta2-adrenoceptor.

Panel A. Washing experiment demonstrating the reversibility of the stimulatory action of the metal-ion complexes.

Panel B. The effect of copper and complexes in the wild-type beta2-AR and in engineered forms of the receptor.

Panel C. Dosis-response analysis of selected copper-chelator complexes on the [F289C;N312C] beta2-AR.

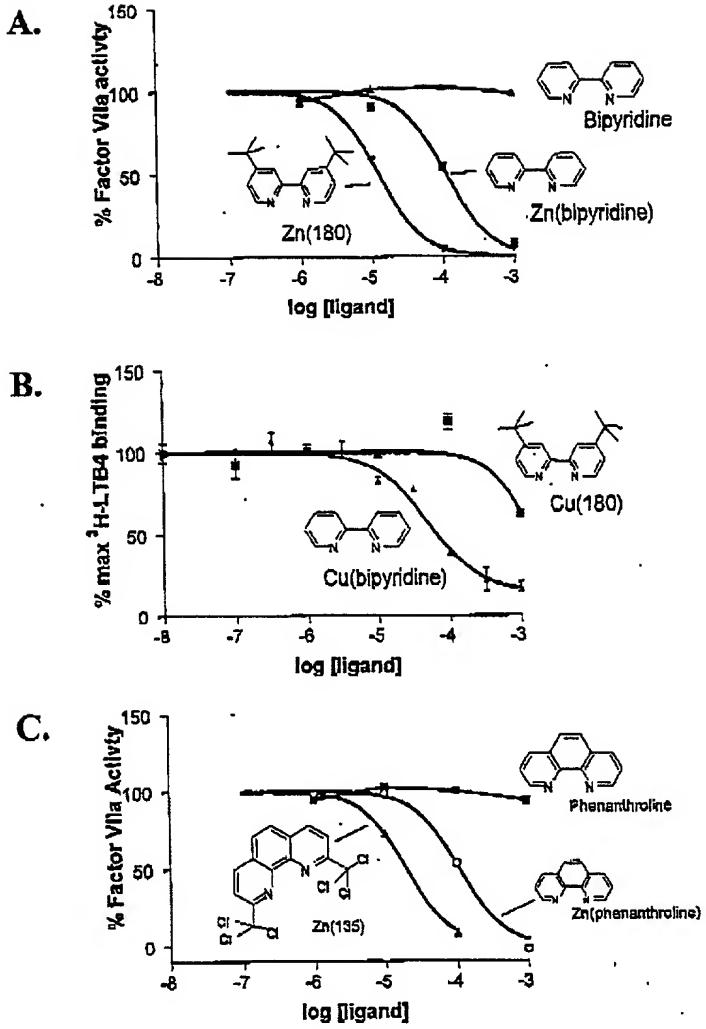

Figur III.4
Structure-activity relationship of antagonistic metal-ion complexes in a soluble protein, the enzyme FVIIa.
A comparison of selected metal-ion complexes on the binding of [3H]-LTB4 and the inhibition of the enzymatic activity of the active form of Factor VII (FVIIa) in COS-7 cells expressing respectively the LTB4 receptor (Panel B) and the FVIIa (Panles A and C). For stucture of the chelators see the Appendix.

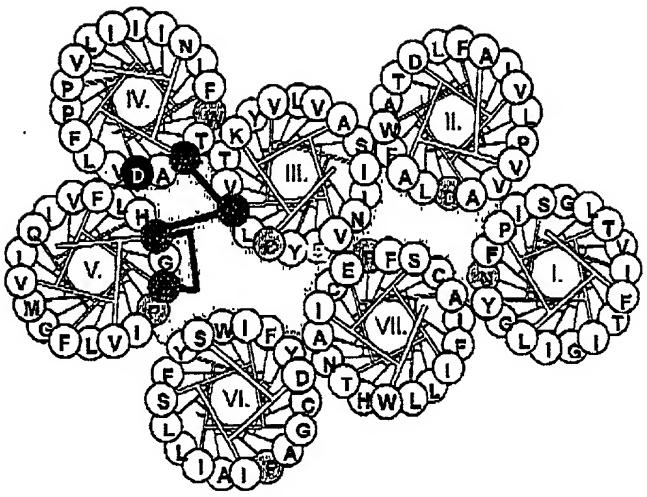

Figur III.5

Structure-based optimization of metal-ion chelators for secondary interactions in the CXCR4 receptor and other biological targets.

Helical wheel diagram for the CXCR4 receptor. The Asp171 residue present in the transmembrane segment IV, and which is considered a major attachment site for the binding of the cyclam chelator is shown in white on black. Positions which in combination are proposed to constitute putative metal-ion binding sites are high-lighted in pairs and in black on dark gray.

Compound	Structure	Name	Provider
62	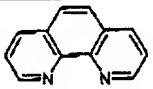	1,10-Phenanthroline	Sigma
92	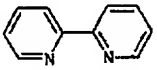	Dipyridine	Sigma
60	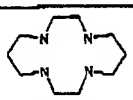	Cyclam	Aldrich
80	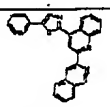	2-(isoquinoline-3-yl)-4-(5-phenyl-oxazol-2-yl)-quinoline	ChemDiv Inc.
83	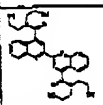	2,2'-di(4-(N,N-(2-hydroxyethyl)carboxamide)quinoline)	ChemDiv Inc.
85	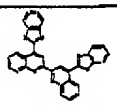	2,2'-di(4-(benzimidazol-2-yl)-quinoline)	ChemDiv Inc.
133	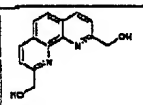	2,9-dimethanol-1,10,phenanthroline	Sigma-Aldrich
134	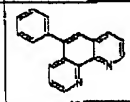	5-phenyl-1,10-phenanthroline	Sigma-Aldrich
135	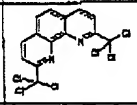	2,9-bis(trichloromethyl)-1,10-phenanthroline	Sigma-Aldrich
175	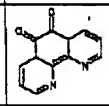	1,10-phenanthroline-5,6-dione	Aldrich
176	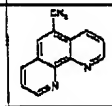	5-methyl-1,10-phenanthroline	Sigma
180	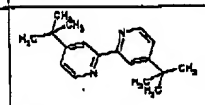	4,4'-Di-tert-butyl-2,2'-dipyridyl	Aldrich
183	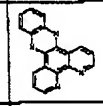	Dipyrido[3,2-a:2',3'-c]phenazine hemhydrate	ABCR GmbH & Co
209	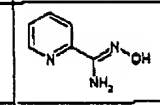	2-pyridylamidoxime	7TM Pharma
210	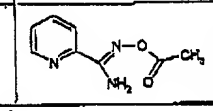	2-pyridylamidoxime, O-acetyl	7TM Pharma

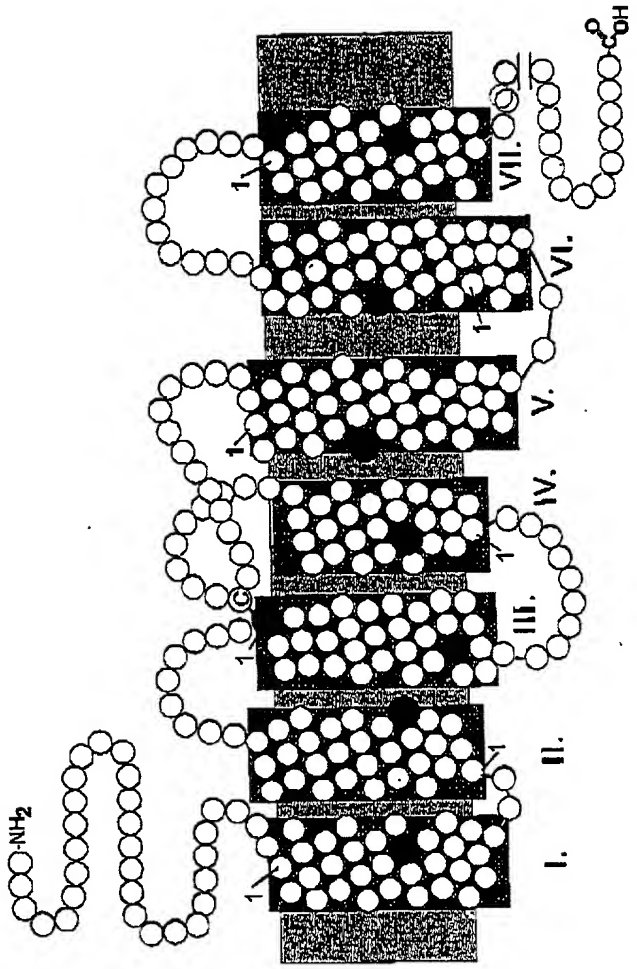
-NH2
I.
II.
III.
IV.
V.
VI.
VII.
COOH
TM-I
TM-II
TM-III
TM-IV
TM-V
TM-VI
TM-VII
AsnI:18
AspII:10
CysIII:01
ArgIII:26
TrpIV:10
ProV:16
ProVI:15
ProVII:17

Figur IV

	Metal ion	Log K_1	Log K_2	Log K_3
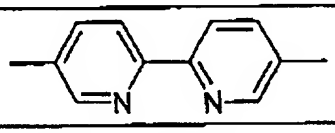	Co^{2+}	6.4	11.3	16.6
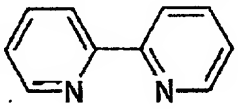	Co^{2+} Ni^{2+} Zn^{2+} Cu^{2+}	5.8 7.0 5.3 8.1	11.3 13.9 9.6 13.6	16.0 16.6 13.3 17.0
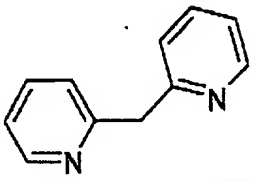	Zn^{2+}	2.8	5.2	
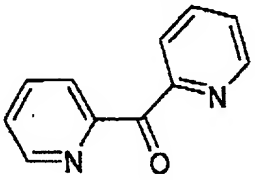	Cu^{2+}	5.1		
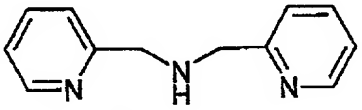	Zn^{2+}	7.6	12.1	
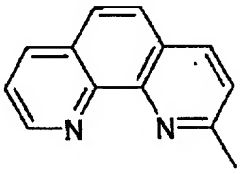	Zn^{2+} Cu^{2+}	5.0 7.4	9.4 13.8	12.7
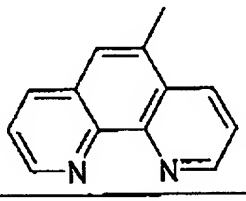	Zn^{2+} Cu^{2+}	6.6 8.6	12.6 15.0	18.3 20.0
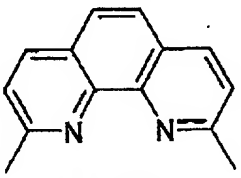	Zn^{2+} Cu^{2+}	4.1 5.2	7.7 11.0	19.1
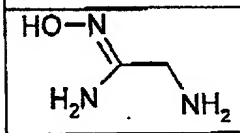	Zn^{2+}	4.1	7.8	9.5

Figur V